Dyes and Pigments 120 (2015) 271–278

Contents lists available at ScienceDirect

Dyes and Pigments

journal homepage: www.elsevier.com/locate/dyepig

Synthesis and characterization of iron oxide pigments through the method of the forced hydrolysis of inorganic salts

Marcelo Müller [a], Juan Carlo Villalba [b], Filipe Quadros Mariani [a], Mariane Dalpasquale [a], Milena Zvolinski Lemos [a], Manuel Fernando Gonzalez Huila [c], Fauze Jacó Anaissi [a, *]

[a] Universidade Estadual do Centro-Oeste, UNICENTRO, R. Simeão Camargo Varela de Sá 03, CEP 85040-080, Guarapuava, PR, Brazil
[b] Faculdade Guarapuava, Departamento de Engenharia, CEP 85015-080, Guarapuava, PR, Brazil
[c] Instituto de Química, Departamento de Química Fundamental, Universidade de São Paulo, Av. Lineu Prestes 748, CEP 05508-000, São Paulo, SP, Brazil

ARTICLE INFO

Article history:
Received 27 December 2014
Received in revised form
14 April 2015
Accepted 20 April 2015
Available online 29 April 2015

Keywords:
Iron oxide nanoparticles
Forced hydrolysis
Synthetic pigments
Characterization
Precursors
Dispersion in white paint

ABSTRACT

Iron oxide hydroxides were synthesized through forced hydrolysis of iron (III) chloride hexahydrate and iron (III) nitrate nonahydrate that as a function of temperature yield different phases characterized by their colors. The tonalities were related to the chemical composition as well as particle size as shown through energy dispersive spectroscopy, thermogravimetric analysis and dynamic light scattering. Iron chloride yielded Akaganèite with different opaque yellow tonalities and a mean particle size of196 (50 °C), 253 (70 °C), 235 (90 °C) and 170 nm (110 °C). The nitrate precursor yielded Goethite with yellow tonalities and particle size of 360 (60 °C) and 318 nm (70 °C), and Hematite with red tonalities and particle size of 262 (90 °C) and 261 nm (110 °C). The test dispersion and coloring of the white paint (water-based) showed an effective coating capacity, chemical and physical stability of the dispersant and iron pigments.

1. Introduction

Iron makes up about 6.3% of the Earth's crust; however it is never found in pure form, but instead, combined with other elements, especially oxygen, yielding iron oxides. These iron compounds possess distinct properties such as coloration, resulting from electron transitions between the *d* (t_{2g} and e_g) orbitals. These colors include yellows and reds, which are responsible for soil colors [1,2].

In living organisms, iron oxides are responsible for the activities of many enzymes, and in this way, they can be applied in biomedicine. Synthetic iron oxides are of great importance in many fields. Some oxides are used as catalysts, in redox processes and as pigments [3–8]. They are used to dye paper, rubber, plastics and cement, paint components, varnishes and enamels, because of the range of colors (yellow, brown, red, etc.) that can be obtained [9].

The colors of synthetic iron oxides differ depending on the method and conditions employed [8–16], as for each oxide or oxide hydroxide phase a specific method is necessary. No reporting was found in the literature regarding the synthesis of different types of iron oxides employing different forced hydrolysis temperatures in order to obtain pigments with different colors.

This article presents the identification of iron oxide hydroxides synthesized at different temperatures of forced hydrolysis (thermohydrolysis), beginning with inorganic precursors iron (III) chloride hexahydrate ($FeCl_3 \cdot 6H_2O$) and iron (III) nitrate nonahydrate ($Fe(NO_3)_3 \cdot 9H_2O$). These syntheses yielded nanoparticles with a slight change in the composition that is responsible for the colors in these oxide hydroxides. The principal properties studied were thermal behavior, size distribution, morphology and chemical composition. The instrumental techniques used for characterization were thermogravimetric analysis, energy dispersive spectroscopy, Raman spectroscopy and X-ray diffractometry. Particle size was determined through dynamic light scattering and X-ray diffractometry. Colors were attributed through electronic spectroscopy.

2. Materials and methods

In the synthesis of the iron oxide pigments (IOPs), iron (III) chloride hexahydrate ($FeCl_3 \cdot 6H_2O$, VETEC) and iron (III) nitrate nonahydrate ($Fe(NO_3)_3 \cdot 9H_2O$, SYNTH) were used. All reactants

* Corresponding author. Tel.: +55 42 3629 8327.
E-mail addresses: anaissi@unicentro.br, fjanaissi@gmail.com (F.J. Anaissi).

http://dx.doi.org/10.1016/j.dyepig.2015.04.026
0143-7208/

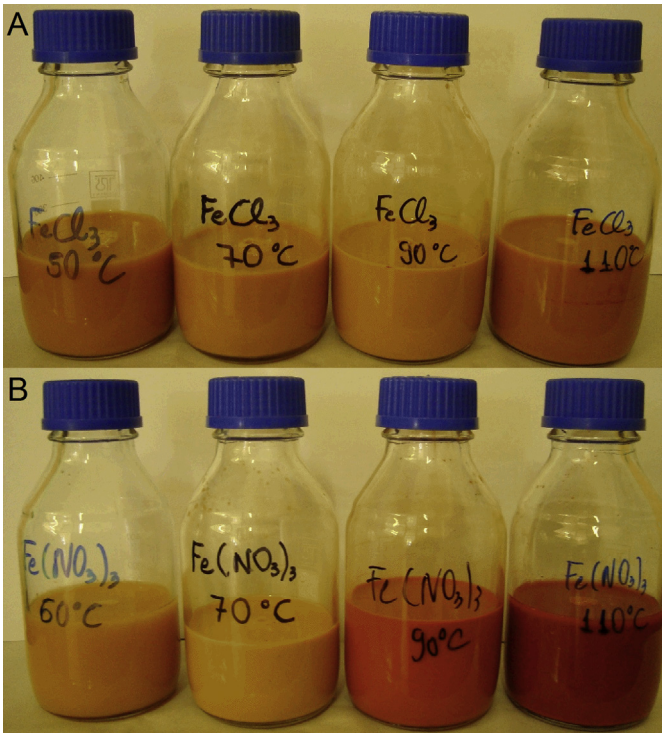

Fig. 1. Photography of the bottles of reactions containing IOPs identified in relation to precursors ($FeCl_3$–$Fe(NO_3)_3$) and their temperatures the forced hydrolysis.

were of analytical grade, and all solutions were prepared with ultrapure water.

2.1. Synthesis of iron oxide pigments – IOPs

Iron chloride (6.76 g) and iron nitrate (10.10 g) were dissolved in 250 mL of water and stored in autoclavable flasks (limit of 150 °C). These solutions were transferred to a thermal reactor (QUIMIS, model Q-819v). Syntheses were carried out at 50 °C, 60 °C, 70 °C, 90 °C and 110 °C for a period of 24 h. This period corresponds to the time necessary for the formation of iron oxide hydroxide crystallites [7]. In the studied condition, iron (III) chloride precipitated at 50 °C, while iron (III) nitrate precipitated at 60 °C. All IOPs were washed with ultrapure water using ultracentrifugation at the speed of 10,000 rpm. The pH of the solutions was monitored and remained constant, with values near 3. Fig. 1 shows photographs of the flasks with their respective suspensions, in which the different colors and their tonalities can be observed. The suspensions were frozen (at −7 °C) and lyophilized, and then the IOPs in powder form were characterized as to their structure, morphology and spectroscopic behavior.

2.2. IOPs dispersion in white paint

In order to verify the compatibility and chemical stability of IOPs, they were dispersed in commercial white water-based paint. The dispersion was carried out in the proportion of 100 mg of IOP in 1 mL of water, and then mixed with 1 mL of white paint.

2.3. Characterization techniques

The thermal behavior of the IOPs was studied with a simultaneous thermal analyzer (TG-DTG-DTA) manufactured by Seiko, model 6300. Samples were heated in alumina pans, and the heating ramp was from 30 to 1200 °C, using a heating ratio of 20 °C/min in a compressed air atmosphere (200 mL/min). Chemical analysis were studied through energy dispersive spectroscopy (EDS), model SwiftED-3000, with a tungsten filament as a source of electrons, operated at 15 kV. X-ray diffractometry (XRD) was performed in a Bruker diffractometer, model D2 Phaser, equipped with a copper cathode (λ = 1.5418 Å), operated at 30 kV, current of 10 mA, with a working window of 2°–90° (2θ) and increment of 0.02 °/s. XRD data were treated with the software EVA (Bruker version 1.1) and indexed according to ICDD-PDF2 2009 cards. Raman spectra were

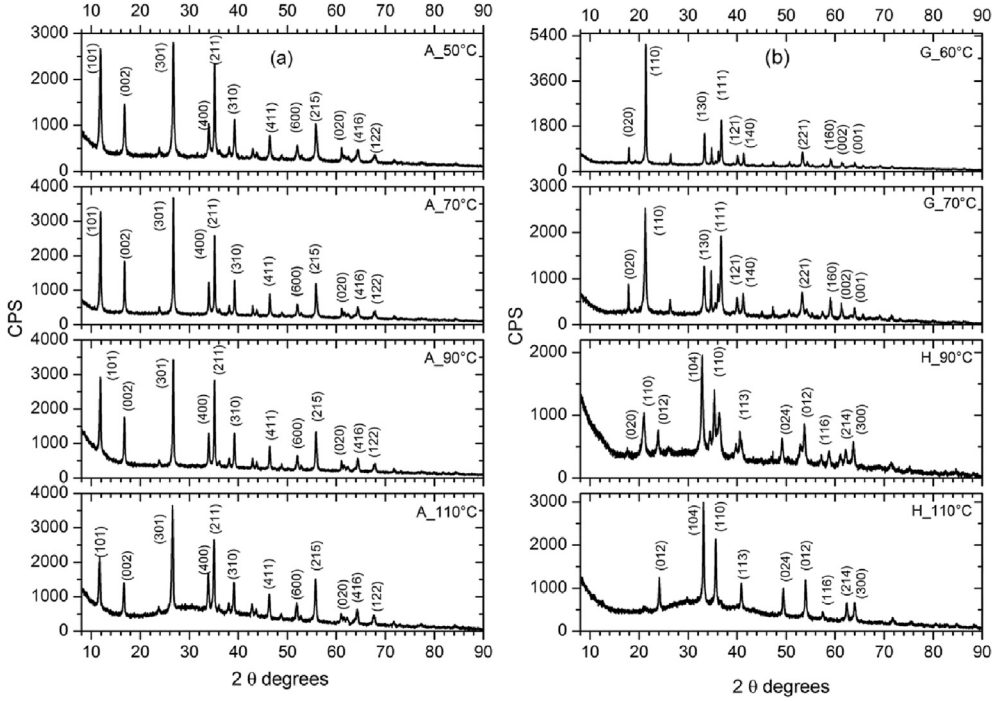

Fig. 2. XRD of the IOPs synthesized according to precursor: A) ferric chloride ($FeCl_3$) and B) ferric nitrate ($Fe(NO_3)_3$).

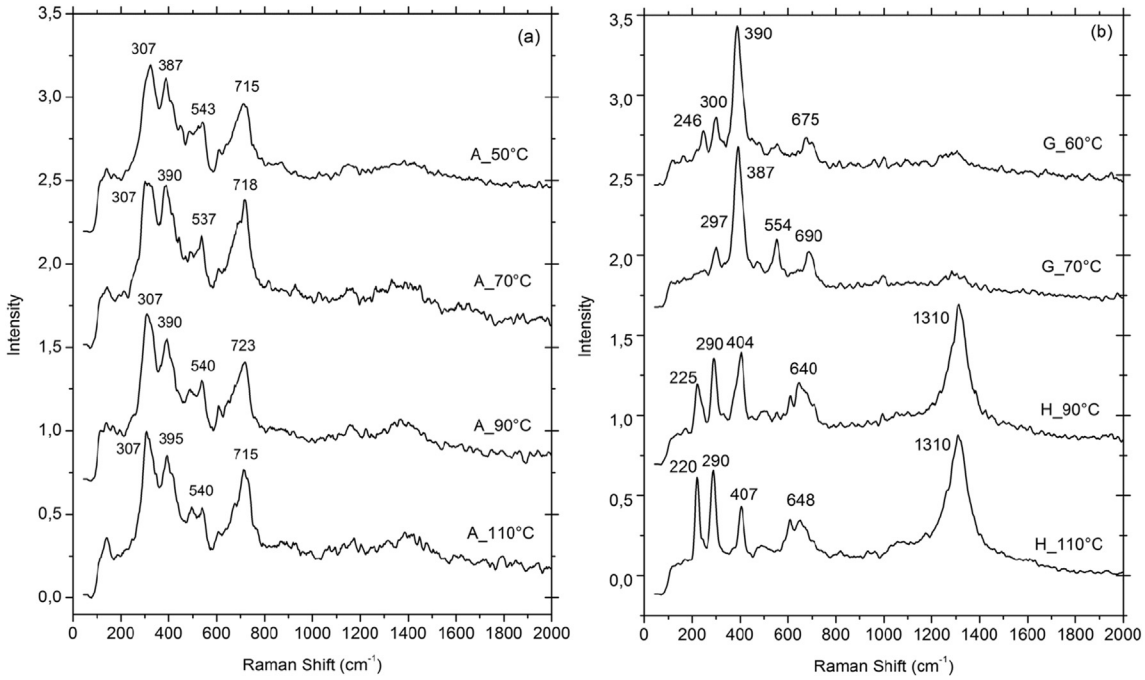

Fig. 3. Raman spectra of the IOPs synthesized according to precursor: A) ferric chloride and B) ferric nitrate.

recorded with a confocal Raman microscope Witec alpha 300, using 532 nm laser excitation and 100× objectives. Laser power was 0.2 mW/cm^2 measured at laser output. Particle size were obtained through dynamic light scattering (DLS) at 20 °C using a Malver Zetasizer Nano, model ZS90 with a detection range of 0.3 nm–6 μm with water as a dispersant. Electronic spectra were obtained using an Ocean Optics spectrophotometer, model USB 2000, equipped with a tungsten-halogen lamp and silicon (UV–Vis, 350–720 nm) and germanium detectors (near IR, 720–1050 nm), linked to a fiber optic accessory and operated in diffuse reflectance mode.

3. Results and discussion

Due to the fact that IOPs prepared with different precursors have distinct colors, different characterization techniques were used for a better understanding of their structural, morphological and spectroscopic properties as well as chemical composition and how it affects their colors and tonalities. The respective oxides were identified through X-ray diffractometry and labeled: Akaganèite (A), Goethite (G)–Hematite (H), followed by the synthesis temperature (for example, A_70 °C).

3.1. X-ray diffractometry (XRD)

X-ray diffractograms showed in Fig. 2A revealed that for the iron chloride [$FeCl_3$] precursor, the principal product was the iron oxide hydroxide [β-FeO(OH)] known as Akaganèite [7,17–19]. The profile is typical of anisotropic crystals, and the Miller indices agree with ICDD (00-016-0123, 00-042-1315 and 00-034-1266) cards. At higher temperatures (90 °C and 110 °C), hematite (α-Fe_2O_3) was also observed, but in low quantities. Characteristic Hematite peaks can be observed at the 38.30° and 41.26° (2θ degree), which correspond to the distances of 2.69 Å and 2.51 Å, respectively.

Fig. 2B shows the XRD for the product obtained through the forced hydrolysis of iron nitrate [$Fe(NO_3)_3$]. Unlike the chloride precursor, at 60 °C and 70 °C, the principal product was Goethite [α-FeO(OH)] [20–22], characterized by the Miller indices (*hkl*) (110/120/310/212/111/121/140) and confirmed through ICDD (01-081-0462 and 00-029-0713) cards. At higher temperatures (90 °C and 110 °C), high crystalline Hematite (α-Fe_2O_3) was the main product. At the temperature of 90 °C, the XRD pattern revealed the presence of low quantities of Goethite [22,23]. The Hematite patterns agreed with ICDD (01-088-2359–00-024-0072) cards and their

Table 1
Analytical data determined by EDS (% elements Fe, O, Cl) and TGA (water) used to estimate the composition of the IOP samples and particle sizes (nm) by DLS.

Sample	Tentative composition by EDS and TGA	Size (nm) ± SD peak 1	Size (nm) peak 2
A_50 °C	$[(\beta\text{-}Fe_{0.43}O_{1.07}(OH)_{1.11}Cl_{0.15}]\cdot 0.25H_2O$	196.50 ± 0.111	n.d.
A_70 °C	$[(\beta\text{-}Fe_{0.63}O_{0.86}(OH)_{0.89}Cl_{0.22}]\cdot 0.26H_2O$	253.30 ± 0.204	3731.0
A_90 °C	$[(\beta\text{-}Fe_{0.34}O_{1.16}(OH)_{1.20}Cl_{0.12}]\cdot 0.20H_2O$	235.40 ± 0.152	3703.1
A_110 °C	$[(\beta\text{-}Fe_{0.42}O_{1.08}(OH)_{1.12}Cl_{0.14}]\cdot 0.24H_2O$	170.50 ± 0.164	1608.1
G_60 °C	$[\alpha\text{-}Fe_{0.43}O_{1.14}(OH)_{1.18}]\cdot 0.15H_2O$	360.20 ± 0.105	n.d.
G_70 °C	$[\alpha\text{-}FeO_{1.16}(OH)_{1,19}]\cdot 0.16H_2O$	318.80 ± 0.046	3221.2
H_90 °C	$[\alpha\text{-}Fe_{0.5}O_{2.22}]\cdot 0.22H_2O$	262.50 ± 0.213	5155.0
H_110 °C	$[\alpha\text{-}Fe_{0.6}O_{2.07}]\cdot 0.20H_2O$	261.60 ± 0.127	5184.3

SD – standard deviation.

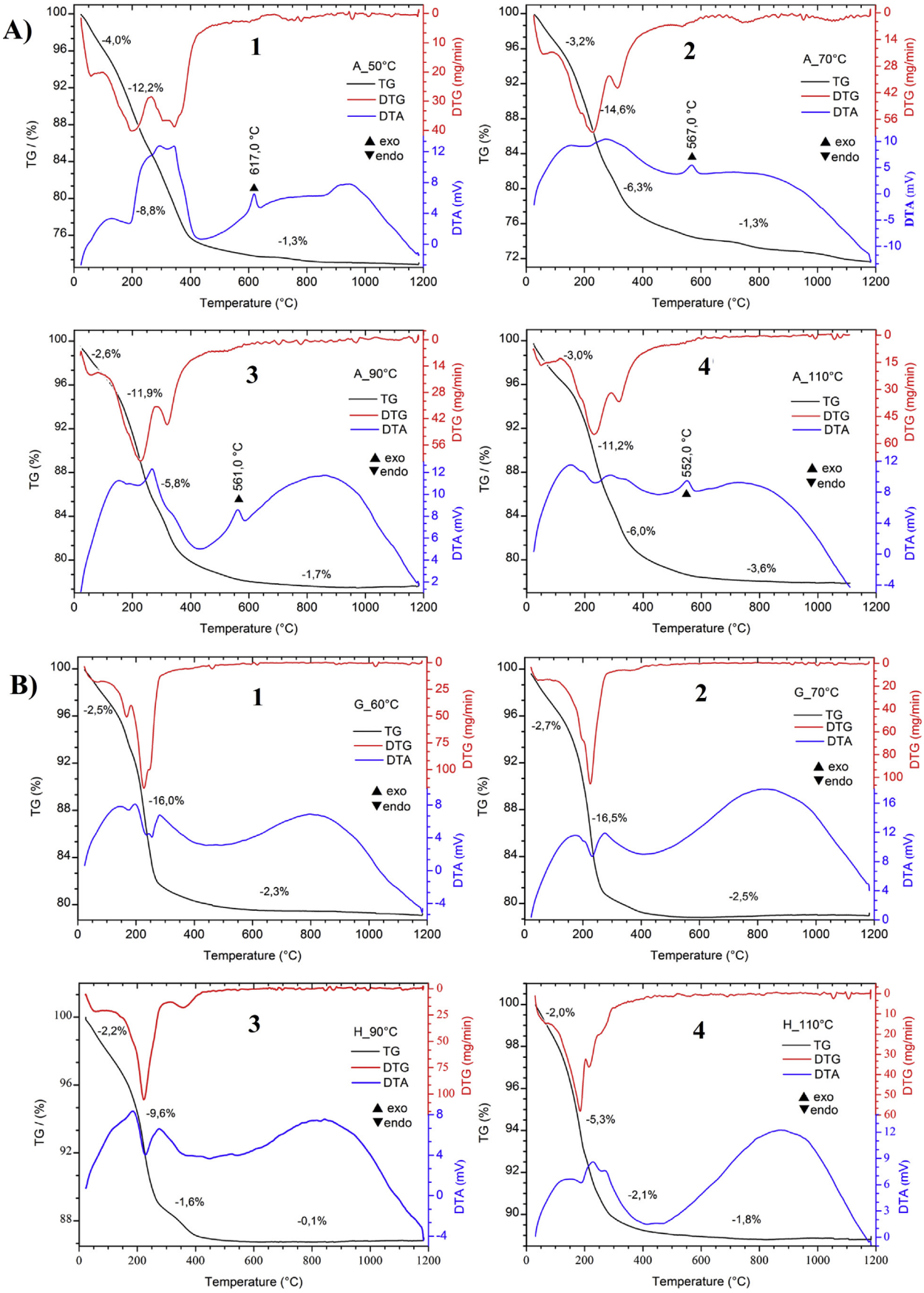

Fig. 4. Curves TG-DTG-DTA of Akaganèite particles obtained precursor: A) ferric chloride, and B) ferric nitrate.

Table 2
Data of the thermal behavior of IOPs: mass loss as a function of temperature range and their assignments.

Temperature range (°C)	Samples/mass loss (%)				Assignment
	A_50 °C	A_70 °C	A_90 °C	A_110 °C	
5–100	4.0	3.2	2.6	3.0	Water (hydration)
100–280	1.2	14,6	11.9	11.2	Water (constitution)
280–450	8.8	6.3	5.8	6.0	Crystallization
450–1200	1.3	1.3	1.5	1.7	Phase transition
	G_60 °C	G_70 °C	H_90 °C	H_110 °C	
25–100	2.5	2.7	2.2	2.0	Water (hydration)
100–300	16.0	16.0	9.6	5.3	Water (constitution)
300–450	–	–	1.6	2.1	Crystallization
300–1100	2.3	1.4	–	–	Crystallization and phase transition
450–1000	–	–	0.1	1.8	Phase transition

characteristic Miller indices were (012/104/110/113/024/116/018/214/300).

The samples A_110 and H_110 exhibited an amorphous halo between 20° and 50° (2θ). This behavior results from the heating temperature [17]. Crystal growth depends on the kinetics and the thermodynamics of the system [24], heating at higher temperatures leads to kinetic dominance, which results in amorphous crystals. As time goes on during the heating process, part of the material formed suffers a dissolution followed by a recrystallization of a new material with greater thermodynamic stability. In this case, we have Akaganèite contaminated with Hematite (greater thermodynamic stability than Akaganèite) in sample A_110, and Hematite (greater thermodynamic stability than Goethite) in sample H_110. This halo is not observed in Akaganèite samples heated at 110 °C for more than 24 h [7].

3.2. Raman spectroscopy

According to Schwertmann and Cornell [17], the characteristic Raman spectra of Akaganèite obtained at 90 °C showed bands at 314, 380, 549–720 cm^{-1}. These bands did not correspond with the materials obtained in this work for the iron chloride reactant at 90 °C. The bands were displaced for temperatures under or above 90 °C (Fig. 3A). This effect could be related to the different shades of these colors. On the other hand, hydrated iron oxide hydroxide showed characteristic band near 383 cm^{-1}, and one or more bands above 476 cm^{-1} that could be related to the modes Fe–O–Fe or OH^- group in the crystal structure [25].

Raman spectra of the iron oxides obtained through iron nitrate precursor showed different vibrational modes (Fig. 3B). Goethite was identified in the samples G_60 °C and G_70 °C. Bands at low frequencies (297–300, 387–397, 554 and 675–690 cm^{-1}) are attributed to octahedral vibration (Fe–O) as described in the literature [26–28]. Raman spectra of the samples H_90 °C and H_110 °C showed bands characteristic of Hematite at 225, 290, 404, 640–1310 cm^{-1}. The band at 1310 cm^{-1} is characteristic of a magnon scattering that is described as an overtone connected to a longitudinal optical phonon (LO) [29].

3.3. Chemical composition (EDS and TG) and particle size

Analytical data were obtained through energy dispersive spectroscopy (EDS) and thermal analysis curve (TG). Table 1 shows the qualitative composition of the iron oxide hydroxides. EDS analysis of the iron chloride precursor at different temperatures (A_50 °C, A_70 °C, A_90 °C, A_110 °C), have iron, chloride and oxygen in their composition, and chloride is an essential component to the formation of Akaganèite [β-FeO(OH)]. Otherwise, samples obtained through the iron nitrate hydrolysis showed just iron and oxygen, in conformity with the chemical formula of Goethite and Hematite.

Table 1 also shows the particles' mean size in nanometers (nm), obtained through dynamic light scattering (DLS) following a bimodal profile. Peaks 1 and 2 showed the mean intensities related to the size. It can be observed that smaller particles are obtained the synthesis carried out at higher temperatures. Peak 1 represents the dominant population (higher percentage) and size at nanometer range, while peak 2 shows the population with bigger size (range of microns), probably due to iron oxide hydroxide clusters.

In general, the iron oxide hydroxides particles obtained through the chloride and nitrate precursors possessed nanometer size. For the $FeCl_3$ precursor at a temperature of 50 °C, the mean size is of 196.5 nm. As temperature increases, the mean size increases, then

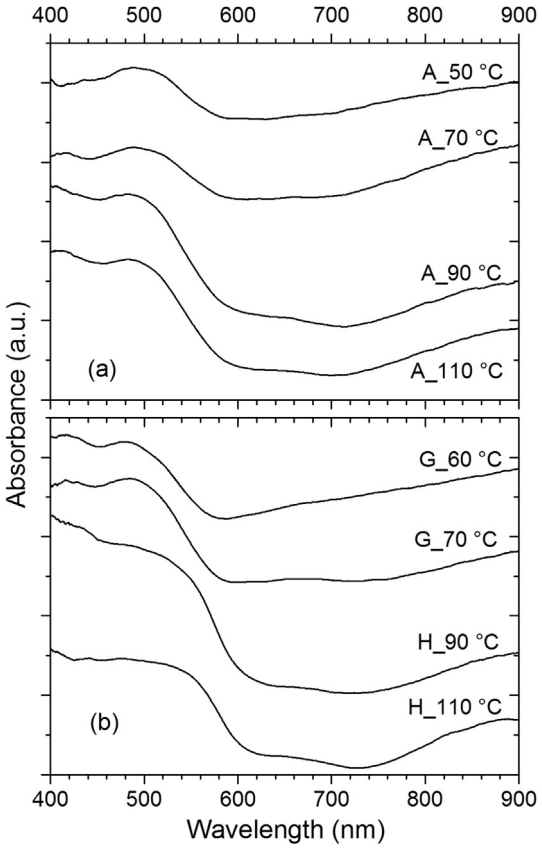

Fig. 5. Electronics spectra (UV–Vis) of the IOPs synthesized according to precursor: A) ferric chloride and B) ferric nitrate.

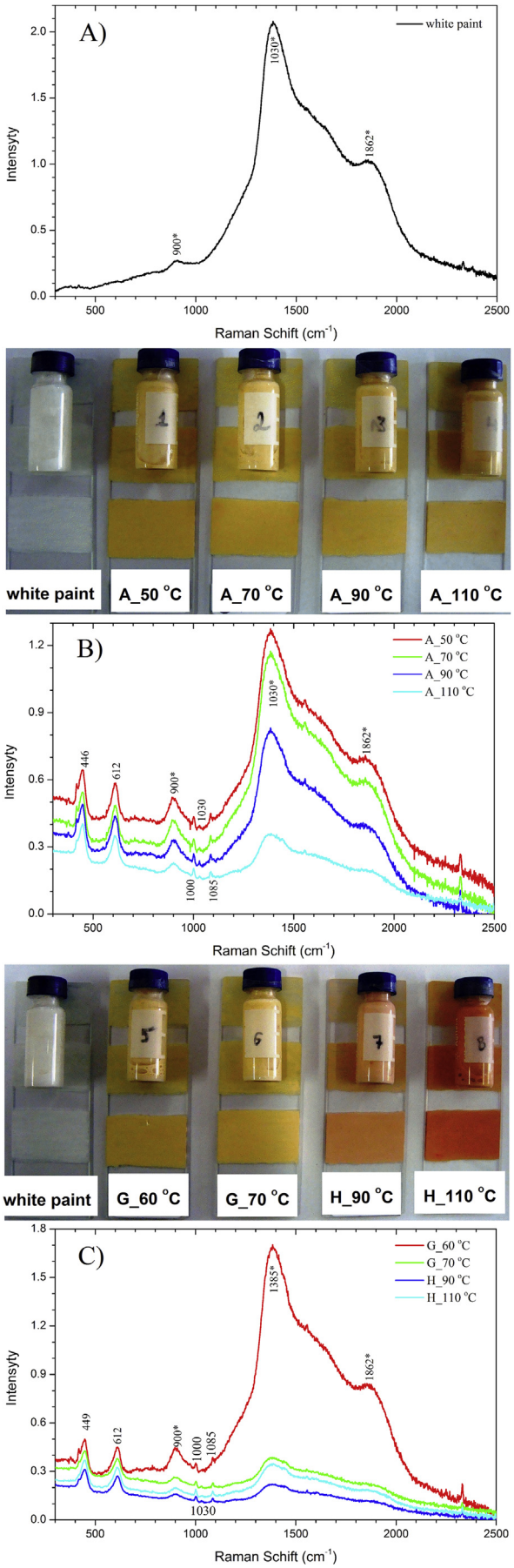

Fig. 6. Raman spectra and photographs of colorful white paint with their IOP: A) white paint, B) ferric chloride and C) ferric nitrate.

above 90 °C it decreases again. For instance, the particles' mean size was 253 nm (70 °C), larger than at 50 °C; at 90 °C it decreased to 235 nm, and at 110 °C, it decreased to 170 nm, which is smaller than the sample obtained at 50 °C. This size indicates that in order to obtain Akaganèite through forced hydrolysis with the smallest particle size, 110 °C is the best temperature.

Samples obtained from iron nitrate also showed particles in the nanometric range, but larger than Akaganèite particles. The mean size for these particles was 360 nm (G_60 °C) and 318 nm (G_70 °C), and the iron oxide hydroxide was identified as Goethite. As the temperature increased, Hematite was formed as the predominant phase and the mean size decreased to 262 nm (H_90 °C) and 261 nm (H_110 °C).

3.4. Thermal analysis curves (TG-DTG-DTA)

Fig. 4A shows the simultaneous thermal analysis curves, each curve shows three or four thermal events. Losses of mass due to chemical or physical processes are shown in Table 2. The first process (endothermic peak, DTA), initial temperature (T_{onset}, 50 °C, DTG curve) was attributed to the leaving of water (hydration and weakly adsorbed), which is a physical phenomenon. After this event, some exothermic events were observed (120–260 °C), due to the dehydroxylation of the iron oxide hydroxides [17,30], which is a chemical process (hydroxyl condensation).

In the range of 400–650 °C, for the Akaganèite samples (Fig. 4A), there was an exothermic process due to the leaving of Cl^- or HCl, followed by the rupture of the Akaganèite crystal structure [5,31]. According to Music et al. [32], with the structure rupture, Akaganèite undergoes a recrystallization yielding Hematite (α-Fe_2O_3). The third event showed a different behavior in terms of temperature peak. The DTA curve revealed a gradual decrease in temperature, for instance, at 617 °C (Fig. 4A.1), 567 °C (Fig. 4A.2), 561 °C (Fig. 4A.3) and 552 °C (Fig. 4A.4).

This decrease is related to the loss of thermal stability of the particles and reflects in the structure of the iron oxyhydroxides since they have different arrangements and chemical bond length (metallic center in the coordination compound). Music et al. [32], reported that this displacement in thermal behavior depends on the methodology adopted, that is, the preparation of the solutions with the addition of other chemical species. In this work, the methodology was changing the temperature of hydrolysis. The fourth and fifth events (750–1100 °C) were due to phase transitions, specifically dehydroxylation.

Fig. 4B shows the thermal behavior characteristics of Goethite and Hematite identified through Raman spectroscopy (Fig. 3B). The events in the TG-DTA curves were attributed to the leaving of water weakly adsorbed on the surface, and dehydroxylation, which occurred at 25–180 °C. After that, in the range of 180–400 °C (Fig. 4B.3 and 4B.4), Goethite was transformed to Hematite [31,33]; the same behavior was observed for the products of 60 °C and 70 °C hydrolysis (Fig. 4B.1 and 4B.2). The fourth event (400–1200 °C) was an exothermic event for the oxide hydroxides (Fig. 4B.3 and 4B.4), attributed to a phase transition, probably Hematite-Maghemite [34].

3.5. ElectronicSpectra (UV–Vis)

The electronic spectra (Fig. 5) shows bands at 350 nm–900 nm, characteristically of UV–Vis absorption involving transitions metals. The IOPs prepared through the chloride and nitrate

precursors showed bands at 480 nm–520 nm and 800 nm–900 nm attributed to the metal-oxygen bonding ($^6A1 \rightarrow {}^4T1$) for the octahedral ion Fe^{+3} [5,17,35].

The variation in the shades of colors is related to the displacement of the absorption band due to the transfer of charge between the ligand (OH^-or O^{2-}) and the Fe^{3+}ion, followed by the loss of symmetry of the Fe^{3+}ion [36]. The shades of colors in the phases Akaganèite, Goethite and Hematite, are explained through the ligand-metal charge transference (LMCT), for instance, the transition (orbital *p* of O^{2-}or OH^-) to the metallic center of Fe^{3+}ion (orbital 3d), which correspond to the transition $6t_{1u} \rightarrow 2t_{2g}$ [37,38].

3.6. Dispersion and coloration of white paint

The white and colored paint were used to paint glass microscope slides (Fig. 6) using three coats of paint. The digital photos show the white paint and its degree of coverage compared to the colored paint. Fig. 6A shows the Raman spectra of white paint. Characteristic bands appeared at 900, 1030 and 1862 cm^{-1} (marked with *) and these were considered as a background for the structural monitoring.

Fig. 6B and C correspond to the Raman spectra of the colored white paint with their IOP. In all Raman spectra (Fig. 6B and C) two characteristic bands of iron oxides (446 and 612 cm^{-1}) are present. Three new bands appear at 1000, 1030 and 1085 cm^{-1}, which may be due to specific interaction between the dispersant phase (white paint) and IOP. These bands will be elucidated in future work.

Fig. 6B shows that the characteristic bands of white paint (marked with *) gradually diminished in intensity as the IOP's particle size decreased (Table 1), i.e., as the degree of paint coverage increases. Fig. 6C shows different (non-linear) behavior. The sample G_60 °C has a profile similar to that of the sample A_50 °C, but the samples G_70 °C, H_90 °C and H_110 °C suffered an abrupt decrease in the relative intensity of the bands of the white paint, thus showing a greater degree of coating and reflectivity.

The test dispersion and coloring of the white paint showed an effective coating capacity, chemical and physical stability of the dispersant and IOP.

4. Conclusions

Through a simple synthesis methodology, it was possible to obtain inorganic pigments, using hydrated iron salts followed by the forced hydrolysis of their solutions at different temperatures. The products had different shades of colors depending on the reactant and temperature. XRD pattern and Raman spectroscopy showed the formation of Akaganèite when the precursor was iron chloride ($FeCl_3$) and Goethite (60 °C and 70 °C) and hematite (90 °C–110 °C) when the reactant was iron nitrate ($Fe(NO_3)_3$).

Thermal analysis confirmed the processes of mass loss of Akaganèite, Goethite and Hematite respectively, associated with the precursors and temperatures used in this work as well as other works found in the literature. Through electronic spectroscopy (UV–Vis) it was possible to distinguish the bands associated with the different shades of colors for each iron oxide hydroxide synthesized. Their colors are a result of differences in the structural arrangement as well as the size of the particles. In this way, they are potentially applicable as inorganic pigments for paints and enamels.

Acknowledgments

The authors would like to thank the Capes Agency (PNPD-1456/2013), Fundação Araucária (Pronex-116-2010/17378), CNPq (Grant No 447902/2014-8) and FINEP (No 01.09.0393.00).

M. Muller expresses gratitude for the master's scholarship granted by CAPES, and M. Z. Lemos is grateful to the PIBIC/CNPq for the undergraduate scholarship.

References

[1] Lee JD. Química inorgânica não tão concisa. São Paulo: Edgard Blucher; 1999.
[2] Jolivet J-P, Tronc E, Chanéac C. Iron oxides: from molecular clusters to solid. A nice example of chemical versatility. Comptes Rendus Geosci 2006;338:488–97.
[3] Lübbe M, Gigler AM, Stark RW, Moritz W. Identification of iron oxide phases in thin films grown on Al_2O_3(0001) by Raman spectroscopy and X-ray diffraction. Surf Sci 2010;604:679–85.
[4] Li Y-S, Church JS, Woodhead AL. Infrared and Raman spectroscopic studies on iron oxide magnetic nano-particles and their surface modifications. J Magn Magn Mater 2012;324:1543–50.
[5] Villalba JC, Constantino VRL, Anaissi FJ. Iron oxyhydroxide nanostructured in montmorillonite clays: preparation and characterization. J Colloid Interface Sci 2010;349:49–55.
[6] Anaissi FJ, Villalba JC, Fujiwara ST, Cótica LF, de Souza CRL, Zamora-Peralta P. Caracterização–propriedades do material coloidal nanoestruturado β-FeOOH/bentonita. Quim Nova 2009;32:2006–10.
[7] Villalba JC, Berezoski S, Cavicchiolli K de A, Galvani V, Anaissi FJ. Structural refinement and morphology of synthetic akaganèite crystals, [β-FeO(OH)]. Mater Lett 2013;104:17–20.
[8] Guskos N, Papadopoulos G, Likodimos V, Patapis S, Yarmis D, Przepiera A, et al. Photoacoustic, EPR and electrical conductivity investigations of three synthetic mineral pigments: hematite, goethite and magnetite. Mater Res Bull 2002;37:1051–61.
[9] Legodi M, Dewaal D. The preparation of magnetite, goethite, hematite and maghemite of pigment quality from mill scale iron waste. Dye Pigment 2007;74:161–8.
[10] Manickavasagam S, Saltiel C, Giesche H. Characterization of colloidal hematite particle shape and dispersion behavior. J Colloid Interface Sci 2004;280:417–30.
[11] Ueda M, Shimada S, Inagaki M. Synthesis of crystalline ferrites below 60 °C. J Eur Ceram Soc 1996;16:685–6.
[12] Ismail H, Cadenhead D, Zaki M. Surface reactivity of iron oxide pigmentary powders toward atmospheric components: XPS and gravimetry of oxygen and water vapor adsorption. J Colloid Interface Sci 1996;183:320–8.
[13] Itoh H, Sugimoto T. Systematic control of size, shape, structure, and magnetic properties of uniform magnetite and maghemite particles. J Colloid Interface Sci 2003;265:283–95.
[14] Narasimhan BR, Prabhakar S, Manohar P, Gnanam F. Synthesis of gamma ferric oxide by direct thermal decomposition of ferrous carbonate. Mater Lett 2002;52:295–300.
[15] Nuñez NO, Morales MP, Tartaj P, Serna CJ. Preparation of high acicular and uniform goethite particles by a modified-carbonate route. J Mater Chem 2000;10:2561–5.
[16] Rodriguez AFR, Gilhermitti MFS, Faria FSEDV, Cunha RM, Santos JG, Oliveira AC, et al. Photoacoustic investigation of maghemite-based nanocomposite. Spectrochim Acta A Mol Biomol Spectrosc 2013;100:72–4.
[17] Cornell RM, Schwertmann U. The iron oxides: structure, properties, reactions, occurrences and uses. 2006.
[18] Zhang Y-X, Jia Y. A facile solution approach for the synthesis of akaganéite (β-FeOOH) nanorods and their ion-exchange mechanism toward As(V) ions. Appl Surf Sci 2014;290:102–6.
[19] Bibi I, Singh B, Silvester E. Akaganéite (β-FeOOH) precipitation in inland acid sulfate soils of south-western New South Wales (NSW), Australia. Geochim Cosmochim Acta 2011;75:6429–38.
[20] Rout K, Dash A, Mohapatra M, Anand S. Manganese doped goethite: structural, optical and adsorption properties. J Environ Chem Eng 2014;2:434–43.
[21] Jaiswal A, Banerjee S, Mani R, Chattopadhyaya MC. Synthesis, characterization and application of goethite mineral as an adsorbent. J Environ Chem Eng 2013;1:281–9.
[22] Pouran HM, Banwart SA, Romero-Gonzalez M. Coating a polystyrene well-plate surface with synthetic hematite, goethite and aluminium hydroxide for cell mineral adhesion studies in a controlled environment. Appl Geochem 2014;42:60–8.
[23] Liang H, Wang Z. Facile synthesis and photocatalytic activity of cocoon-like hollow hematite nanostructures. Mater Lett 2013;96:12–5.
[24] Nielsen AE. Kinetics of precipitation. New York: Pergamon Press; 1964.
[25] Savoye S, Legrand L, Sagon G, Lecomte S, Chausse A, Messina R, et al. Experimental investigations on iron corrosion products formed in bicarbonate/carbonate-containing solutions at 90 °C. Corros Sci 2001;43:2049–64.
[26] Von Aderkas EL, Barsan MM, Gilson DFR, Butler IS. Application of photoacoustic infrared spectroscopy in the forensic analysis of artists' inorganic pigments. Spectrochim Acta A Mol Biomol Spectrosc 2010;77:954–9.
[27] De Faria DLA, Venâncio Silva S, de Oliveira MT. Raman microspectroscopy of some iron oxides and oxyhydroxides. J Raman Spectrosc 1997;28:873–8.

[28] Chattopadhyay A, Bandyopadhyay N, Das AK, Panigrahi M. Oxide scale characterization of hot rolled coils by Raman spectroscopy technique. Sci Mater 2005;52:211–5.
[29] McCarty KF. Inelastic light scattering in α-Fe_2O_3: phonon vs. magnon scattering. Solid State Commun 1988;68:799–802.
[30] Meunier A. Clays. Springer; 2005.
[31] Liu H, Chen T, Zou X, Qing C, Frost RL. Thermal treatment of natural goethite: thermal transformation and physical properties. Thermochim Acta 2013;568:115–21.
[32] Musić S, Krehula S, Popović S. Thermal decomposition of β-FeOOH. Mater Lett 2004;58:444–8.
[33] Ruan HD, Frost RL, Kloprogge JT. The behavior of hydroxyl units of synthetic goethite and its dehydroxylated product hematite. Spectrochim Acta A Mol Biomol Spectrosc 2001;57:2575–86.
[34] Darezereshki E. One-step synthesis of hematite (α-Fe_2O_3) nano-particles by direct thermal-decomposition of maghemite. Mater Lett 2011;65:642–5.
[35] Chmielarz L, Kowalczyk A, Michalik M, Dudek B, Piwowarska Z, Matusiewicz A. Acid-activated vermiculites and phlogophites as catalysts for the DeNOx process. Appl Clay Sci 2010;49:156–62.
[36] Schwidder M, Kumar M, Klementiev K, Pohl M, Bruckner A, Grunert W. Selective reduction of NO with Fe-ZSM-5 catalysts of low Fe content I. Relations between active site structure and catalytic performance. J Catal 2005;231:314–30.
[37] Cotton FA, Wilkinson G, Gaus PL. Basic inorganic chemistry. John Wiley Sons, Inc; 1995.
[38] Hidaka M, Takeuchi K, Wijesundera RP, Kumara LSR, Sugihara S, Momoshima N, et al. Structural and electronic properties of iron oxides in the celadon glazes (II). Cerâmica 2012;58:534–41.